Orbital: The Electronic Journal of Chemistry
journal homepage: www.orbital.ufms.br
ISSN 1984-6428

| Vol 5 | | No. 3 | | Special Issue 2013 |

Full Paper

Adsorption of Crystal Violet Dye from Aqueous Solution onto Zeolites from Coal Fly and Bottom Ashes

Tharcila C. R. Bertolini*, Juliana C. Izidoro, Carina P. Magdalena, Denise A. Fungaro

Chemical and Environmental Center, Nuclear and Energy Research Institute, Av. Prof. Lineu Prestes, 2242, CEP 05508-000, São Paulo, Brazil.

Article history: Received: 27 March 2013; revised: 05 June 2013; accepted: 22 July 2013. Available online: 10 October 2013.

Abstract: The adsorption of the cationic dye Crystal Violet (CV) over zeolites from coal fly ash (ZFA) and bottom ash (ZBA) was evaluated. The coal fly ash (CFA) and the coal bottom ash (CBA) used in the synthesis of the zeolites by alkaline hydrothermal treatment were collected in Jorge Lacerda coal-fired power plant located at Capivari de Baixo County, in Santa Catarina State, Brazil. The zeolitic materials were characterized predominantly as hydroxy-sodalite and NaX. The dye adsorption equilibrium was reached after 10 min for ZFA and ZBA. The kinetics studies indicated that the adsorption followed the pseudo-second order kinetics and that surface adsorption and intraparticle diffusion were involved in the adsorption mechanism for both the adsorbents. The equilibrium data of ZFA was found to best fit to the Langmuir model, while ZBA was best explained by the Freundlich model. The maximum adsorption capacities were 19.6 mg g^{-1} for the CV/ZFA and 17.6 mg g^{-1} for the CV/ZBA.

Keywords: crystal violet; coal fly ash; coal bottom ash; zeolite; adsorption

1. INTRODUCTION

The manufacture and use of synthetic dyes for dyeing fabrics has become an industry solid. It is estimated that around 700,000 tons of dyes are produced annually around the world. Of this amount about 20% is unloaded the industrial wastes without previous treatment. However, their use has become a matter of serious concern to environmentalists. Synthetic dyes are highly toxic causing negative effects on all life forms because they present sulfur, naphthol, vat dyes, nitrates, acetic acid, surfactants, enzymes chromium compounds and metals such as copper, arsenic, lead, cadmium, mercury, nickel, cobalt and certain auxiliary chemicals [1-2].

The crystal violet (CV) dye is a synthetic cationic dye and transmits violet color in aqueous solution. It is also known as Basic Violet 3, gentian violet and methyl violet 10B, belonging to the group of triarylmethane [3]. This dye is used extensively in the textile industries for dying cotton, wool, silk, nylon, in manufacture of printing inks and also the biological stain, a dermatological agent in veterinary medicine [3-4]. The CV is toxic and may be absorbed through the skin causing irritation and is harmful by inhalation and ingestion. In extreme cases, can lead to kidney failure, severe eye irritation leading to permanent blindness and cancer [5-6]. Therefore, removal of this dye from water and wastewater is of great importance.

Various methods of treatment exploited through the years by industries for removing colorants include physicochemical, chemical, and biological methods, such as flocculation, coagulation, precipitation, adsorption, membrane filtration, electrochemical techniques, ozonation, and fungal decolorization [7]. However, due to the fact that effluents contain different dyes, and these dyes contain complex structures, is very difficult to treat using conventional methods [8].

The adsorption is one of the most effective processes of advanced wastewater treatment, which industries employ to reduce hazardous pollutants present in the effluents. This is a well-known and superior technique to other processes for removal of dyes from aqueous worldwide due to initial cost, operating conditions and simplicity of design [9]. Currently, the most common procedure involves the use of activated carbon as adsorbent for this purpose

*Corresponding author. E-mail: thacolachite@yahoo.com.br

by offering greater adsorption capacities. However, due to their relatively high cost, many lower-cost adsorbents have been investigated as adsorbent for removing contaminants from wastewater. The low-cost adsorbents can be made from waste materials, thus collaborating with the environment and also getting economic advantages. A wide variety of low-cost adsorbents have been prepared from different materials utilizing industrial, biomass, and municipal wastes [10-14].

Thermoelectric power stations produce a great quantity of residues from combustion of coal. The major solid waste by-product of thermal power plants based on coal burning is fly ash. The coal-fired power plants in the southern of Brazil produce approximately 4 Mt of ash per year, of which 65–85% is fly ash and 15–35% bottom ash. The main uses of fly ash include pozzolanic cement, paving, bricks, etc., but only 30% of what is produced in the year are recycled [15-16]. The bottom ash are previously disaggregated and transported to the settling ponds through pumping hydraulic [17]. This may lead to environmental problems through leaching of toxic substances present in the ashes. One way to reduce the environmental impact of the disposal of these wastes is to expand its utilization. An alternative solid waste is recycling of the transformation of the coal ash at a low cost adsorbent able to remove toxic substances from contaminated waters [18-22].

The coal ash can be converted into zeolites due to their high contents of silicon and aluminum, which are the structural elements of zeolites. The most common method involves a hydrothermal treatment with sodium hydroxide [23-24]. This technique of recycling coal ashes has been extensively investigated for water treatment due to its large specific surface area and cation exchange capacity, low cost, and mechanical strength [25-29].

The aim of this work was to evaluate the efficiency of synthesized zeolites from Brazilian coal fly and bottom ashes as adsorbent in the removal of basic dye crystal violet from aqueous solutions. Batch kinetic experiments were performed to provide appropriate equilibrium times. The Langmuir and Freundlich isotherm models were used to model the isotherm data for their applicability.

2. MATERIAL AND METHODS

All chemicals used in this study were of analytical grade. Crystal Violet (CV) which was used as a model cationic dye in this work was purchased from Proton-Research and considered as purity 100%. The general characteristics of CV are summarized in Table 1 and the chemical structure is in Fig. 1. A stock solution (5.0 g. L^{-1}) was prepared with deionized water (Millipore Milli-Q) and the solutions for adsorption tests were prepared by diluting. The samples of coal fly and bottom ashes were obtained from Jorge Lacerda coal-fired power plant located at Capivari de Baixo County, in Santa Catarina State, Brazil.

Table 1. General characteristics of CV dye.

Chemical name	**Crystal Violet**
Color index	CI 42555
λ_{max} (nm)	590
Molar mass (g mol^{-1})	408
Chemical formula	$C_{25}H_{30}N_3Cl$

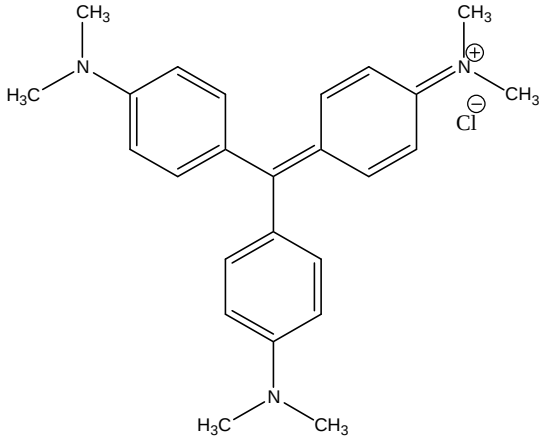

Figure 1. Chemical Structure of CV.

Zeolite synthesis

The zeolite was synthesized by hydrothermal activation of 20 g of coal fly (CFA) or coal bottom ashes (CBA) at 100 °C in 160 mL of 3.5 mol L^{-1} NaOH solution for 24 h. The zeolitic material was repeatedly washed with deionized water to remove excess sodium hydroxide until the washing water had pH ~ 10, then it was dried at 50 °C for 12 h [30]. The zeolitic products obtained were labeled as ZFA and ZBA for zeolite prepared with fly ash and bottom ash, respectively.

Adsorbents characterization

The mineralogical compositions of the samples (ZFA and ZBA) used as adsorbents and the samples saturated with dye (CV/ZFA and CV/ZBA) were determined by X-ray diffraction analyses (XRD) with

an automated Rigaku multiflex diffractometer with Cu anode using Co Kα radiation at 40 kV and 20 mA over the range (2θ) of 5–80°with a scan time of 0.5°/min.

The chemical composition of CBA and ZBA, in the form of major oxides, was determined by X-ray fluorescence (XRF) in a Rigaku RIX- 3000 equipment. The bulk density and the specific surface area of CBA and ZBA was determined by a helium picnometer (Micromeritcs Instrument Corporation — Accupyc 1330) and by a BET Surface Area Analyser (Quantachrome Nova — 1200), respectively. Prior to determination of the specific surface area, samples were heated at 423.15 K for 12 h to remove volatiles and moisture in a degasser (Nova 1000 Degasser). The BET surface areas were obtained by applying the BET equation to the nitrogen adsorption data.

For the cation exchange capacity (CEC) measurements, the samples CBA and ZBA were saturated with sodium acetate solution (1 mol L^{-1}), washed with 1L of distilled water and then mixed with ammonium acetate solution (1 mol L^{-1}) [31]. The sodium ion concentration of the resulting solution was determined by optical emission spectrometry with inductively coupled plasma — ICP-OES (Spedtroflame — M120).

The pH and the conductivity were measured as follows: the bottom ashes and zeolite bottom ashes (0.25 g) were placed in 25 mL of deionized water and the mixture was stirred for 24 h in a shaker at 120 rpm (Ética — Mod 430). After filtration, the pH of the solutions was measured with a pH meter (MSTecnopon — Mod MPA 210) and the conductivity was measured with a conductivimeter (BEL Engineering - Mod W12D).

The determination of the zero point charge (pH_{PZC}) of ZFA and ZBA was carried out as follows: the samples (0.1 g) were placed in 50 mL of potassium nitrate (0.1 mol L^{-1}) and the mixtures were stirred for 24 h in the mechanical stirrer (Quimis – MOD Q-225M) at 120 rpm. The initial pH of solutions was adjusted to the values of 2, 4, 10, 11, 12 and 13 by addition of 0.1 and 1 mol L^{-1} HCl or 3 mol L^{-1} NaOH solution. The difference values between the initial and final pH (pH Δ) were placed in a graph in function of the initial pH. The point x where the curve intersects the y = 0 is the pH of PCZ.

The content of loss of ignition (LOI) of coal bottom ashes in this study were calculated according to the weight loss of the samples subjected to heating at 1050°C for 4 h in a muffle furnace and expressed in percentage. The mass of the material used was 0.5 g.

The chemical composition and the some physicochemical properties (bulk density, BET area, total and cation exchange capacity, pH) of CFA and ZFA have been described in a previous paper [26].

Adsorption studies

The adsorption was performed using the batch procedure. Kinetic experiments were carried out by agitating 0.25 g of adsorbent with 25 mL of dye solution with initial concentration of 185 mg L^{-1} at room temperature (25 ± 2 °C) at 120 rpm for 1-12 min for both adsorbents. The collected samples were then centrifuged (3000 rpm during 30 min for ZFA and during 10 min for ZBA) and the concentration in the supernatant solution was analyzed using a UV spectrophotometer (Cary 1E, Varian) by measuring absorbance at λ = 590 nm and pH = 5.

The adsorption capacity (mg·g^{-1}) of adsorbents was calculated using Eq. 1:

$$q = \frac{V(C_o - C_f)}{M} \qquad (1)$$

where q is the adsorbed amount of dye per gram of adsorbent, C_0 and C_f the concentrations of the dye in the initial solution and equilibrium, respectively (mg L^{-1}); V the volume of the dye solution added (L) and M the amount of the adsorbent used (g).

The efficiency of adsorption (or removal) was calculated using the equation:

$$R = 100\frac{(C_o - C_f)}{C_o} \qquad (2)$$

where R is the efficiency of adsorption (%), C_o is the initial concentration of dye (mg L^{-1}), C_f is the equilibrium concentration of dye at time t (mg L^{-1}).

Adsorption isotherms were carried out by agitating 0.25 g of zeolite with 25 mL of crystal violet over the concentration ranging from 24.4 to 236 mg L^{-1} for ZFA and 24.4 to 247.9 mg L^{-1} for ZBA till the equilibrium was achieved. The adsorption capacity (mg g^{-1}) of adsorbents was calculated using a Eq.1.

3. RESULTS AND DISCUSSION

Characterization of the adsorbents material

The X-ray diffractograms of ZFA and ZBA are

shown in Fig. 2 and 3, respectively. The identification and interpretation of PXRD patterns of the materials are prepared by comparing the diffraction database provided by "International Centre for Diffraction Data/Joint Committee on Power Diffraction Standards" (ICDD/JCPDS). The phases in zeolitic materials were hydroxysodalite (JCPDS 31-1271) and NaX (JCPDS 38-0237) with peaks of quartz (JCPDS 85-0796) and mullite (JCPDS 74–4143) of ashes that remained after the treatment. The mineralogical composition of ash used as raw material for the synthesis of zeolites depends on the geological factors related to the formation and deposition of coal and its combustion conditions.

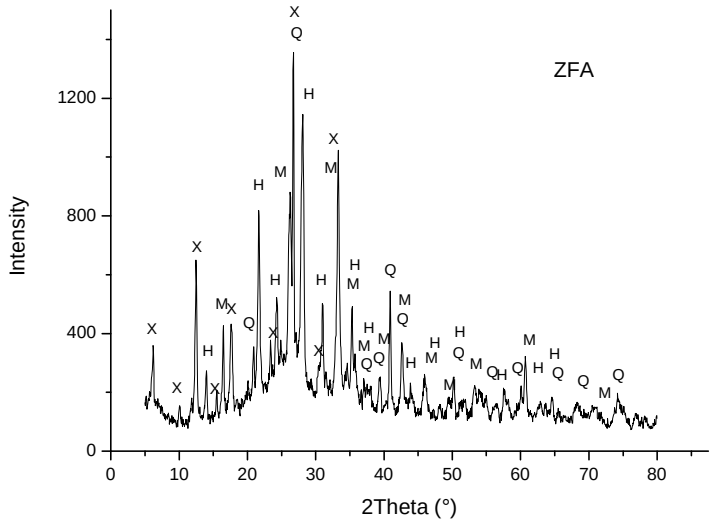

Figure 2. XRD Patterns of ZFA (Q = Quartz, M = Mullite, H = Hydroxysodalite zeolite, X = NaX zeolite).

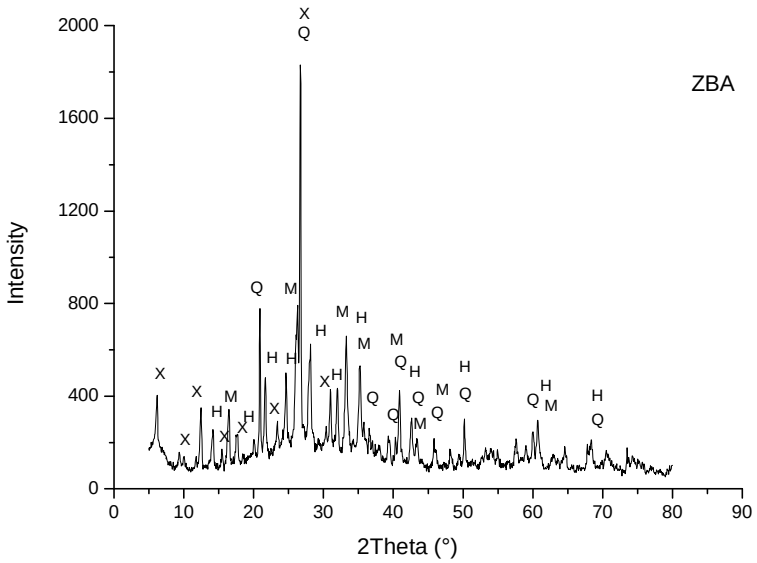

Figure 3. XRD Patterns of ZBA (Q = Quartz, M = Mullite, H = Hydroxysodalite zeolite, X = NaX zeolite).

The diffraction patterns of the zeolites obtained before and after adsorption of CV are shown in Fig. 4. The structural parameters of saturated ZFA and ZBA were very close to those of the corresponding ZFA and ZBA before adsorption. The crystalline nature of the zeolites remained intact after adsorption of molecules CV.

The chemical composition of CBA and ZBA determined by X-ray fluorescence (XFR) is shown in Table 2. The chemical compositions of CFA and ZFA have been described in detail in previous paper [26].

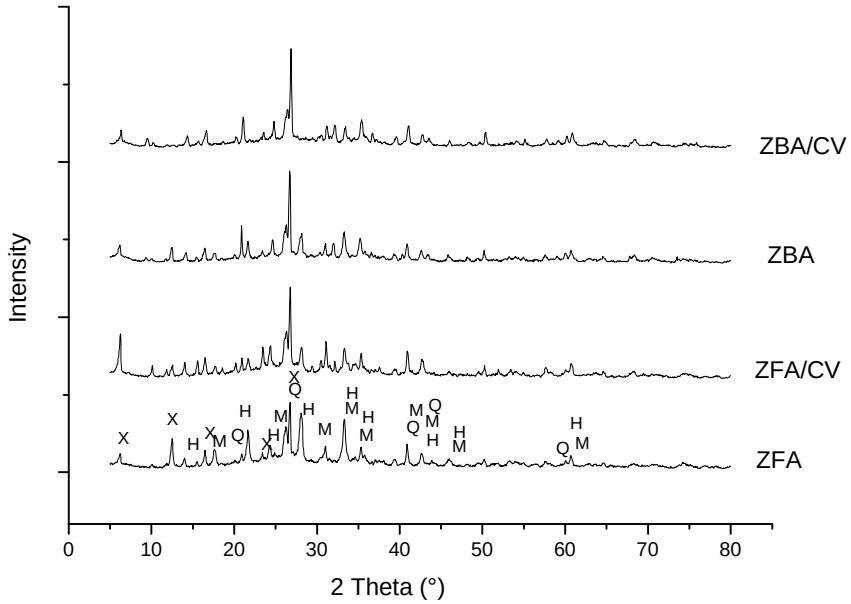

Figure 4. XRD Patterns of zeolites and zeolites saturated with dye (Q = Quartz, M = Mullite, H = Hydroxy-sodalite zeolite, X = NaX zeolite).

Table 2. Chemical composition of CBA and ZBA.

Elements (wt. %)	CBA	ZBA
SiO_2	49.6	35.1
Al_2O_3	27	32.9
Fe_2O_3	10.9	16.1
Na_2O	1.9	7.7
CaO	1.8	3.2
K_2O	4.4	0.7
TiO_2	1.9	2.4
SO_3	0.7	0.3
MgO	1.3	1.3
ZnO	0.03	0.03
ZrO_2	0.03	0.04
SiO_2/ Al_2O_3	1.84	1.06

The main constituents of CBA are silica (SiO_2), alumina (Al_2O_3), and ferric oxide (Fe_2O_3). Quantities below 5 wt.% of K_2O, CaO, TiO_2, SO_3 and MgO are also observed.

The main constituents observed for CBA were the same of CFA: 50.3 wt.% of SiO_2, 29.8 wt.% of Al_2O_3, and 6.70 wt.% of Fe_2O_3. It has found also oxides of calcium, titanium, sulfur and other compounds in amounts below 5 wt.%. The SiO_2/Al_2O_3 ratio was 1.69 and 1.84 for CFA and CBA, respectively, indicating good source to synthesize zeolites [32].

The coal and its ash generated in Jorge Lacerda coal-fired power plant were analyzed by Silva et al 2010. The results indicated that coal is bituminous-type, highly volatile (C/A). Samples of fly ash showed the following ranges of the main elements of higher concentration (wt.%): 57.98 – 60.10 of SiO_2, 22.98-26.97 of Al_2O_3 and 4.67-8.01 of Fe_2O_3. For samples of bottom ash ranges were (wt.%): 46.14 to 61.95 of SiO_2, 19.20 to 23.88 of Al_2O_3 and 5.38 to 7.81 of Fe_2O_3.

The chemical composition found for ZBA is mainly silica, alumina, iron oxide and sodium oxide (Table 2). The main constituents for ZFA were 36.6 wt.% of SiO_2, 38.0 wt.% of Al_2O_3, 8.30 wt.% of Fe_2O_3 and 6,90 wt.% of Na_2O. A significant amount of Na element is incorporated in the final products due to hydrothermal treatment with NaOH solution.

The SiO_2/Al_2O_3 ratio for zeolites is associated to the cation exchange capacity. The values observed for ZFA was 0.96 and the value calculated for ZBA was 1.06 (Table 2). The SiO_2/Al_2O_3 ratios for the zeolites are lower than the values of raw fly and bottom ashes. The hydrothermal treatment contributed to the increase in the cation exchange capacity of these materials. The zeolitic material that exhibit lower the ratio SiO_2/Al_2O_3, have higher the cation exchange capacity.

Some physicochemical properties of coal bottom ash and its zeolitic material are given in Table 3. The same physicochemical properties for CFA and ZFA are presented in previous paper [26].

Table 3. Physicochemical properties of coal bottom ash (CBA) and zeolite from coal bottom ash (ZBA).

Properties physicochemical	CBA	ZBA
Bulk density (g cm^{-3})	1.79	2.43
BET surface area (m^2 g^{-1})	5.33	84.9
Loss of ignition (%)	9.33	-
pH in water	7.6	8.4
pH_{PZC}[a]	-	7.3
Condutivity (µS cm^{-1})	110	367
CEC (meq g^{-1})[b]	0.109	1.19

(a) point of zero charge; (b) cation exchange capacity

The bulk density values ranged from 1.79 to 2.43 g cm^{-3} for ash and zeolites. Kreuz [33] found value of bulk density 1.81 g cm^{-3} for bottom ash from thermal power plant Jorge Lacerda, which is very close to the value found for the ash of this study.

The specific surface area value of the zeolite bottom ash was approximately 16 times greater than those of its precursor ash. The specific surface area value for ZFA was also higher (134.3 m^2 g^{-1}) than the value for CFA (9.6 m^2 g^{-1}). This area increase is due to the crystallization stage zeolitic on the smooth spherical particles of the ash after the hydrothermal treatment.

The CEC values of the ash are much low, and is similar to the value reported in the literature [34]. The CEC values of ZBA and ZFA were 10 and 50 times higher than CBA and CFA, respectively, due to hydrothermal treatment. Therefore, the synthesized zeolites can be used as good cation exchanger.

The pH of the coal ash is directly related to the availability of macro and micro nutrient and indicates whether coal ash is acidic or alkaline in nature. Based on the pH, coal ash has been classified into 3 categories, namely; slightly alkaline 6.5–7.5; moderately alkaline 7.5-8.5 and highly alkaline >8.5 [35]. The pH values of fly ash (8.0) and bottom ash (7.6) indicates that ashes were moderately alkaline in nature. This alkalinity is justified by the presence of compounds formed by the cations K^+, Na^+, Ca^{2+} and Mg^{2+} combined with carbonates, oxides or hydroxides [34]. The pH of zeolitic materials increased due to hydrothermal treatment with NaOH solution.

The conductivity values found for synthesized zeolites were higher than those of raw ashes. This increase is explained by presence of exchangeable cations in the structures of the zeolites formed by the hydrothermal treatment.

Depoi et al. [36] found a conductivity value of 119 µS cm^{-1} for bottom ash, which is accordance with the present study.

The point of zero charge (PZC) is defined as the pH at which the surface of the adsorbent has neutral charge. The pH_{PCZ} adsorbents depends on several factors such as the nature of crystallinity, Si/Al ratio, impurity content, temperature, adsorption efficiency of electrolytes, degree of adsorption of H^+ and OH^-, and, therefore, it must vary adsorbent for adsorbing [37]. The value of pH_{PZC} of ZBA (Table 3) was lower than the pH in water indicating that the surface presented negative charge in aqueous solution (pH> pH_{PZC}). The value of the pH_{PZC} of ZFA obtained in this study was 6.5. This value is lower than the pH and the surface of ZFA also showed negative charge.

The data of loss on ignition of coal ash may indicate the combustion efficiency of a thermoelectric power plant. The high levels of this property make it difficult the synthesis of zeolites, as the non-reactive phase may be a lesser amount during conversion. The loss on ignition is usually indicative of the presence of unburned carbon and mineral phases stable at high temperatures [38]. The loss on ignition values found for CFA and CBA were 15.1% and 9.33%, respectively. According to the obtained values of loss on ignition of Brazilian fly ash was suggested that the Jorge Lacerda Thermal Power Plant has a low efficiency [26].

Kinetics studies

Figure 5 shows the effect of contact time on adsorption process of CV on ZFA and on ZBA. The efficiency of dye removal was increased as the agitation time increased until equilibrium. The adsorption equilibrium with ZFA and ZBA were reached at 10 min. The process shows the removal of 71% and 50% with ZFA e ZBA, respectively.

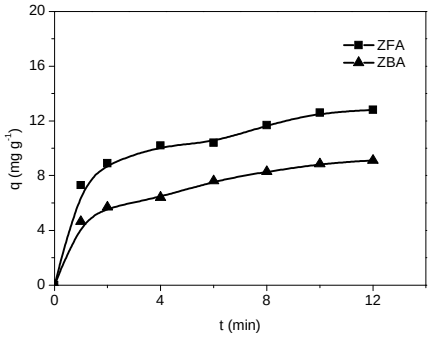

Figure 5. Effect of contact time on the adsorption of CV onto ZFA and ZBA.

Kinetic models

In order to investigate the adsorption processes of CV onto adsorbents, pseudo-first order and pseudo-second order kinetic models were applied to the experimental data. The pseudo-first-order kinetic model, proposed by Lagergren, has been widely used to predict the dye adsorption kinetics. The dye adsorption kinetics following the pseudo-first-order model is given by [39]:

$$\frac{dq}{dt} = k_1(q_e - q) \qquad (3)$$

where q and q_e represent the amount of dye adsorbed (mg g^{-1}) at any time t and at equilibrium time, respectively, and k_1 represents the adsorption rate constant (min^{-1}). Integrating Eq. (3) with respect to boundary conditions $q = 0$ at $t = 0$ and $q = q$ at $t = t$, then Eq. (3) becomes:

$$\log_{10}(q_e - q) = \log_{10} q_e - k_1 t / 2{,}303 \qquad (4)$$

Thus the rate constant k_1 (min^{-1}) can be calculated from the plot of log (q_e-q) *vs.* time *t*.

The kinetic data were further analyzed using a pseudo second- order relation proposed by [40] which is represented by:

$$\frac{dq}{dt} = k_2(q_e - q)^2 \qquad (5)$$

where k_2 is the pseudo-second-order rate constant (g mg^{-1} min^{-1}) and q_e and q represent the amount of dye adsorbed (mg g^{-1}) at equilibrium and at any time *t*. Separating the variables in Eq. (6) gives

$$\frac{dq}{(q_e - q)^2} = k_2 dt \qquad (6)$$

Integrating Eq. (6) for the boundary conditions $t = 0$ to $t = t$ and $q = 0$ to $q = q$ gives

$$\frac{t}{q} = \frac{1}{k_2 q_e^{\,2}} + \frac{1}{q_e} t \qquad (7)$$

A plot *of t/q vs. t* gives the value of the constants k_2 (g mg^{-1} min^{-1}), and also q_e (mg g^{-1}) can be calculated.

Because the above two equations cannot give definite mechanisms, the intraparticle diffusion model was tested. According to Weber and Morris [41], an intraparticle diffusion coefficient k_{dif} is defined by the equation:

$$q_t = k_{dif} t^{1/2} + C \qquad (8)$$

where k_{dif} is the intraparticle diffusion rate constant (mg g^{-1} $min^{-1/2}$), and C is the intraparticle diffusion constant (mg g^{-1}). The constants k_{dif} and C can be obtained, respectively, from the slope and intercept of the plot of qt versus $t^{1/2}$. The relative values of C give an idea about the boundary layer thickness, i.e., the larger the intercept value, the greater the boundary layer effect [41-43].

Figure 6 shows the fitting results using (a) first-order kinetic model; (b) second-order kinetic model, and (c) diffusion model. The parameters for all models are presented in Table 4.

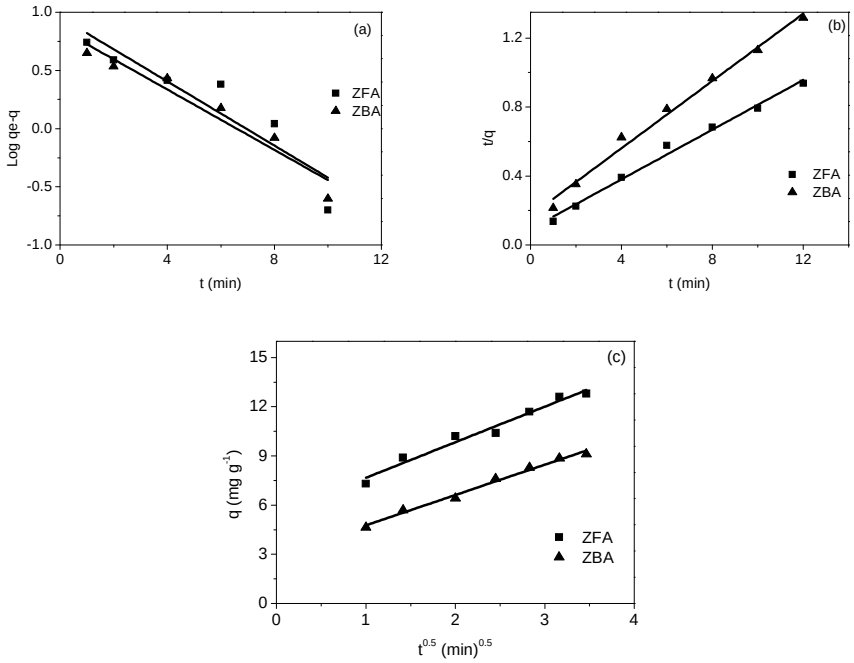

Figure 6. Comparison of kinetic models, and diffusion model of CV adsorption on ZFA and ZBA (a) first-order kinetics; (b) second-order kinetics; (c) diffusion model.

Table 4. Kinetic parameters for CV removal onto ZFA and ZBA.

Adsorbents	Pseudo- first order				
	k_1 (min) $^{-1}$	q_e calc (mg g^{-1})	q_e exp (mg g^{-1})	R_1	
ZFA	3.17 x 10^{-1}	9.10	12.8	0.927	
ZBA	2.99 x 10^{-1}	7.16	9.11	0.970	
	Pseudo- second order				
	k_2 (gmg^{-1}min^{-1})	h (mg g^{-1}min^{-1})	q_e calc (mg g^{-1})	q_e exp (mg g^{-1})	R_2
ZFA	5.59 x 10^{-2}	10.8	13.9	12.8	0.996
ZBA	5.60 x 10^{-2}	5.88	10.2	9.11	0.995
	Intraparticle diffusion				
	C	k_{dif} (mg g^{-1}min$^{-0.5}$)	R_i		
ZFA	5.49	2.17	0.986		
ZBA	2.92	1.85	0.995		

The experimental q_e values (Table 4) did not agree with the calculated ones obtained from the linear plots, indicating that the pseudo-first order model does not reproduce the adsorption kinetics of CV onto ZFA and ZBA. The k_2 and qe determined from the model are presented in Table 4 along with the corresponding correlation coefficients. The values of the calculated and experimental q_e are close to ZFA and also to ZBA, and the calculated correlation coefficients (R) are also very close to unity. Hence, the pseudo-second order model better represented the adsorption kinetics.

The linearity of the fitting lines obtained from the application of the diffusion model (Fig. 6c) points to the presence of intraparticle diffusion in the system. However, the fact that the lines do not pass through the origin of the plots indicates that, although intraparticle diffusion may be involved in the adsorption process, it was not the rate-controlling step [41].

A comparison of calculated and measurement results for kinetic of CV adsorption onto ZFA and ZBA are shown in Fig. 7a and 7b, respectively. As can be seen, the pseudo-first order model underestimates the adsorption and the pseudo second-order kinetic model provides the best correlation for both adsorption processes.

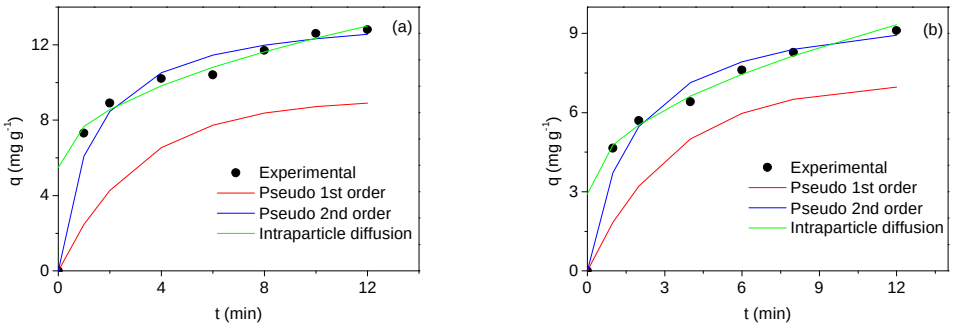

Figure 7. Comparison between the measured and modeled time profiles for adsorption of CV for (a) ZFA and (b) ZBA.

Adsorption equilibrium

In adsorption in a solid–liquid system, the distribution ratio of the solute between the liquid and the solid phases is a measure of the position of equilibrium. The preferred form of depicting this distribution is to express the quantity q_e as a function of C_e at a fixed temperature and an expression of this type is termed an adsorption isotherm [44]. The quantity q_e is the amount of solute adsorbed per unit weight of the solid adsorbent, and C_e is the concentration of solute remaining in the solution at equilibrium.

The analysis of the isotherm data is important to develop an equation which accurately represents the results and which could be used for design purposes [39]. In the present study, Langmuir,

Freundlich and Dubinin-Radushkevich (*D-R*) models were used to describe the equilibrium data.

The Langmuir isotherm assumes that the sorption takes place at specific homogeneous sites within the adsorbent [45]. The linear form of Langmuir isotherm is represented by the Eq. 9:

$$\frac{C_e}{q_e} = \frac{1}{Q_o b} + \frac{C_e}{Q_o} \qquad (9)$$

where C_e is the equilibrium concentration (mg L^{-1}), q_e the amount adsorbed at equilibrium (mg g^{-1}), Q_0 the adsorption capacity (mg g^{-1}) and, b is the energy of adsorption (Langmuir constant, L mg^{-1}). The values of Q_0 and b were calculated from the slope and intercept of the linear plots C_e q_e^{-1} *versus* C_e which give a straight line of slope $1/Q_0$ that corresponds to complete monolayer coverage (mg g^{-1}) and the intercept is $1/Q_0 b$.

The Freundlich isotherm is derived by assuming a heterogeneous surface with a non-uniform distribution of heat of adsorption over the surface [46]. The logarithmic form is shown as Eq. 10:

$$\log q_e = \log K_f + \frac{1}{n}\log C_e \qquad (10)$$

where K_F [(mg g^{-1} (L $mg^{-1})^{1/n}$)] and n are the Freundlich constants related to adsorption capacity and adsorption intensity of adsorbents, respectively. They were calculated from the intercept and slope of the plot log qe versus log C_e.

Langmuir and Freundlich isotherms do not give any idea about adsorption mechanism. The Dubinin–Radushkevich isotherm (*D-R*) is generally applied to express the adsorption mechanism (physical or chemical) with a Gaussian energy distribution onto a heterogeneous surface [47]. This isotherm model is more general than Langmuir isotherm because it does not assume a homogeneous surface or a constant adsorption potential and is related to the porous structure of the adsorbent. The linear form of *D-R* isotherm equation is represented as:

$$\ln q_e = \ln K_{DR} - \beta\, \epsilon^2 \qquad (11)$$

where K_{DR} is the theoretical saturation capacity (mol g^{-1}), β is a constant related to the mean free energy of adsorption per mole of the adsorbate (mol^2 J^{-2}), Є is Polanyi potential which is mathematically represented as:

$$\varepsilon = \ln(1 + 1/C_e)\; x\; RT \qquad (12)$$

where, C_e is the equilibrium concentration of adsorbate in solution (mol L^{-1}), R is the gas constant (J mol^{-1} K^{-1}) and T is the absolute temperature (K). The *D-R* model constants, K_{DR} and β, can be determined from the intercept and slope of linear plot of ln q_e versus ϵ^2, respectively.

The constant β gives an idea about the mean free energy E (kJ mol^{-1}) of adsorption per molecule of the adsorbate when it is transferred to the surface of the solid from infinity in the solution and can be calculated from the relationship:

$$E = \frac{1}{\sqrt{-2\beta}} \qquad (13)$$

If the magnitude of E is between 8 and 16 kJ mol^{-1}, the adsorption process is supposed to proceed via ion-exchange or chemisorption, while for values of E<8 $kJmol^{-1}$, the adsorption process is of physical nature [48].

Figures 8 and 9 show the adsorption isotherms of CV on ZFA and ZBA, respectively, where the experimental values and curves achieved from the values estimated by the Langmuir, Freundlich and D-*R* models are presented. The adsorption efficiency was between 78 to 99% ZFA and 65 to 96% for ZBA at equilibrium time.

Giles et al. [49] state that isotherm shapes are largely determined by the adsorption mechanism, and thus can be used to explain the nature of adsorption. The adsorption isotherm for solution may be classified into four main classes relating to their shapes termed S, L, H and C and subgroups 1, 2, 3, 4 or max. The equilibrium isotherms for the system CV/ZFA showed sigmoidal curve in the class with the corresponding behavior L2. In processes where such isotherms are obtained, the adsorption of solute onto the adsorbent proceeds until a monolayer is established; the formation of further layers is not possible in this case [50].

Comparing the isotherm for the system CV/ZBA with those given by Giles et al [49], L4 type of isotherm (Langmuir type with two layers) appears to fit the adsorption data well. After the first degree of saturation of the surface, further adsorption takes place on new surface.

Figures 10 and 11 illustrate the Langmuir, Freundlich and *D-R* plots for the removal of CV by ZFA and ZBA, respectively. The Langmuir, Freundlich, and *D-R* isotherm constants are given in Table 5 along with the corresponding correlation coefficients.

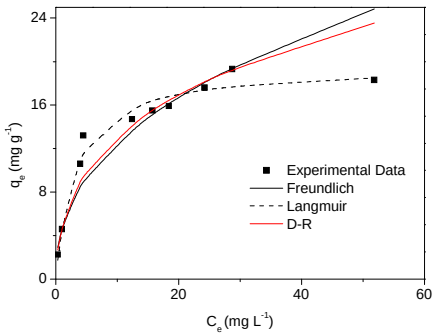

Figure 8. Adsorption isotherm of CV onto ZFA (T = 25 ^{o}C; t agitation = 10 min).

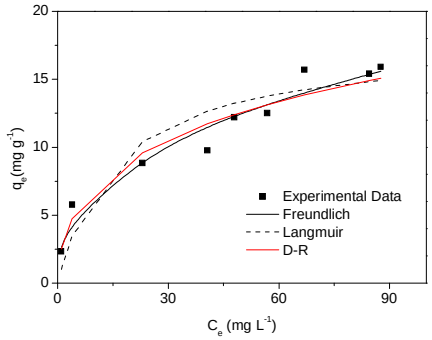

Figure 9. Adsorption isotherm of CV onto ZBA (T = 25 ^{o}C; t agitation = 10 min).

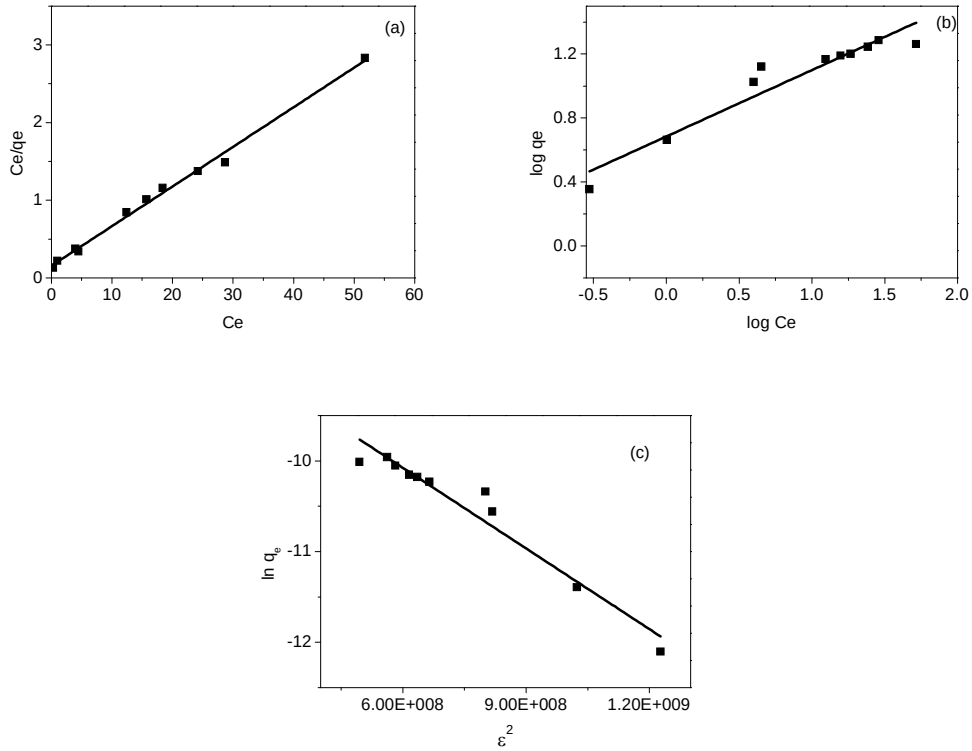

Figure 10. Langmuir (a), Freundlich (b) and D-R (c) plots for adsorption of CV onto ZFA.

Table 5. Parameters of the models of Langmuir isotherm, Freundlich and *D-R* for the CV dye on adsorbents and values and Chi-square (χ^2)

	Adsorbents	
Lagmuir	ZFA	ZBA
Q_o (mg g^{-1})	19.6	17.7
B (L mg^{-1})	0.329	0.0630
R	0.997	0.961
X^2	0.706	4.53
Freundlich		
K_F (mg g^{-1})(L mg^{-1})$^{1/n}$	4.83	2.66
N	2.41	2.53
R	0.959	0.981
X^2	4.42	0.869
D-R		
β (mol^2 J^{-2})	2.96 x 10^{-9}	3.03 x 10^{-9}
K_{DR} (mol g^{-1})	2.49 x 10^{-4}	1.39 x 10^{-4}
E (kJ mol^{-1})	13.0	12.8
R	0.973	0.983
X^2	3.01	0.966

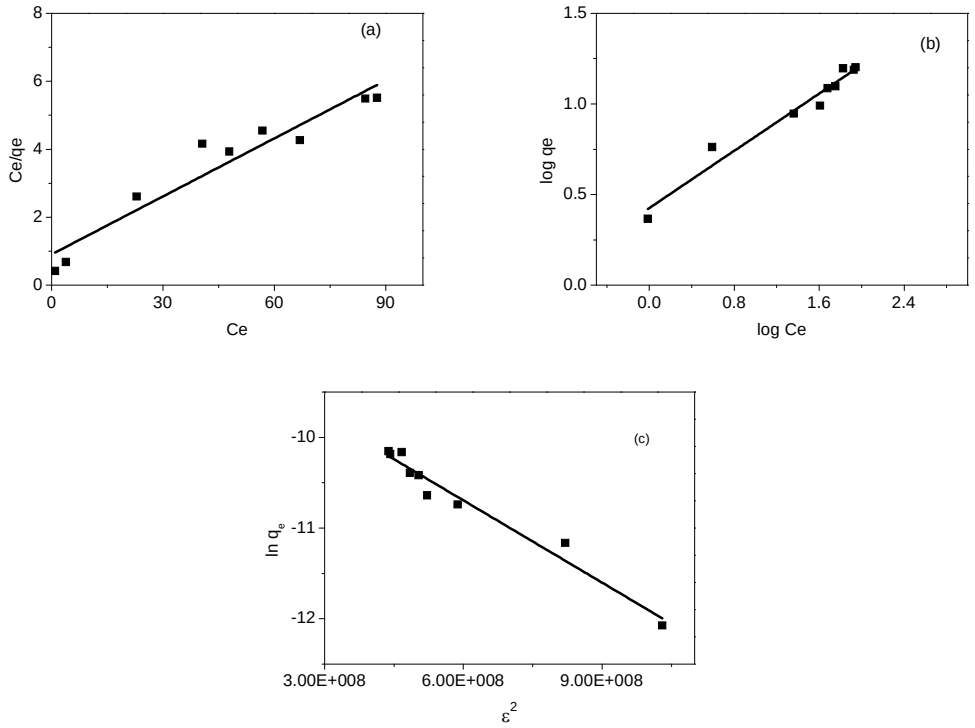

Figure 11. Langmuir (a), Freundlich (b) and *D-R* (c) plots for adsorption of CV onto ZBA.

By comparing the correlation coefficient values obtained from the Langmuir, Freundlich and D-R isotherm models, it can be concluded that the Langmuir isotherm model is more suitable for CV/ZFA while the experimental data obtained for CV/ZBA were fitted well by the Freundlich isotherm model. This may be due to both homogeneous and heterogeneous distribution of active sites on the surface of the ZBA. Both energy distributions induce single and multilayer adsorption. These might occur simultaneously or subsequently by order of time, both in a random manner [51].

The adsorption for the system CV/ZFA obeys Langmuir isotherm better, indicating predominantly homogeneous distribution of active sites on the ZFA surface, since the Langmuir equation assumes that the adsorbent surface is energetically homogeneous.

The Freundlich isotherm constant, n, gives an idea for the favorability of the adsorption process. The value of n should be less than 10 and higher than unity for favorable adsorption conditions. As can be seen from Table 5, the n values for ZFA and ZBA were in the range of 1-10, indicating that the adsorption is a favorable process. By evaluating the *D-R* isotherm model, the mean adsorption energy, *E*, values were found to be 13.0 kJ mol^{-1} for ZFA and 12.8 kJ mol^{-1} for ZBA, suggesting that the adsorption mechanisms of CV onto zeolitic materials are chemical in nature.

The non-linear regression Chi-square (X^2) test was employed as a criterion for the fitting quality due to the inherent bias resulting from linearization of isotherm models. Therefore, it is necessary to analyze the data set using the Chi-square test to confirm the best fit isotherm for the adsorption system combined with the values of the correlation coefficient. This statistical analysis is based on the sum of the squares of the differences between the experimental and model calculated data, of which each squared difference was divided by the corresponding data obtained by calculating from models [52]. The Chi-square can be represented by

$$\chi^2 = \sum \frac{(q_e \exp - q_e calc)^2}{q_e calc} \qquad (14)$$

where $q_e$exp is the equilibrium capacity of the adsorbent obtained from experiment ($mg \cdot g^{-1}$), and $q_e$calc is the equilibrium capacity obtained by calculating from the model ($mg \cdot g^{-1}$). A low value of X^2 indicates that experimental data fit better to the value from the model.

Table 5 also shows the values obtained in non-linear test or Chi-square (X^2). The values of regression coefficients, *R* and the linear error functions, X^2, are in agreement to one another. The

lower value of X^2 confirmed statistically a better fit to the Langmuir isotherm for the CV/ZFA system and the Freundlich isotherm for the CV/ZBA system.

The maximum adsorption of capacity of CV, according Langmuir, was about 10% higher on the zeolite ZFA than on the zeolite ZBA, not being a very significant difference. The result of performance of the ZFA was expected because this material will have particles sizes smaller than the zeolite from coal botton ash due granulometric characteristics of the ash sample that served as raw material. Thus, decreasing the particle size increases the externa surface area, which means increasing the number of active sites available for adsorption of the adsorbate and thus increases the efficiency of adsorption [53].

Adsorbents like zeolites consist primarily of silicon and aluminium oxides, whose hydroxylated surface develop negative charges in aqueous solution. The adsorption of CV on the zeolite of coal ash will occurs by electrostatic attraction between the negatively charged sites of the adsorbent and the positively charged dye molecules ($=N^+(CH_3)_2$) and also by cation exchange.

Table 6 lists a comparison of maximum monolayer adsorption capacity of CV on various adsorbents. A close look at the values displayed reveals that the present adsorbents (ZFA and ZBA) have a maximum CV dye uptake value comparable with the reported values in some cases. The adsorption capacity varies, and it depends on the characteristics of the individual adsorbent and the initial concentration of the adsorbate. However, the present experiments are conducted to find the technical applicability of the low-cost adsorbents to treat CV.

Table 6. Comparison of the maximum adsorption of capacities of CV dye onto various adsorbents

Adsorbents	Q_o (mg g^{-1})	References
Fly ash	74.6	[54]
Bottom ash	12.1	[55]
Sepiolite	77.0	[56]
Sulphuric acid	85.8	[5]
Activated carbon	19.8	[57]
ZFA	19.6	This study
ZBA	17.6	This study

4. CONCLUSION

The present study showed that is possible to convert coal ash into zeolitic materials by alkaline hydrothermal treatment. The X-ray diffraction analysis demonstrated that hydroxy-sodalite and NaX zeolites were formed after the synthesis. These zeolites synthesized from fly ash (ZFA) and bottom ash (ZBA) are effective adsorbents for removal the cationic dye crystal violet from aqueous solution. The pseudo-second order model provides the best correlation of the experimental data for both adsorbents and intraparticle diffusion is involved in the adsorption process, but it is not the only rate-limiting step. The equilibrium data fit with the Langmuir isotherm for ZFA and the Freundlich isotherm for ZBA. The adsorption capacity for ZFA was found to be 19.6 mg g^{-1} and for ZBA 17.6 mg g^{-1}. The use of the southern Brazilian coal ash generated in power plants for the production of zeolites can constitute an alternative and noble use for a residue which has contributed to the degrading of wide areas.

5. ACKNOWLEDMENTS

The authors are grateful to Conselho Nacional de Desenvolvimento Científico e Tecnológico (CNPq), Coordenação de Aperfeiçoamento de Pessoal de Nível Superior (CAPES) for supporting this study and Jorge Lacerda coal-fired power plant for providing coal ashes samples.

6. REFERENCE AND NOTES

[1] Kant, R. *Nat. Sci.* **2012**, *4*, 22. [CrossRef]

[2] Carneiro, P. A.; Pupo Nogueira R. F.; Zanoni, M. V. B. *Dye. Pigment*. **2007**, *74*, 127. [CrossRef]

[3] Adak, A.; Bandyopadhyay, M.; Pal, A. *Sep. Purif. Technol.* **2005**, *44*, 139. [CrossRef]

[4] Ayed, L.; Chaieb, K.; Cheref, A. *World J. Microbiol. Biotechnol.* **2009**, *25*, 705. [CrossRef]

[5] Senthilkumaar, S.; Kalaamani, P.; Subburaam, C. V. *J. Hazard. Mater*. **2006**, *136*, 800. [CrossRef]

[6] Mittal, A.; Mittal, J.; Malviya, A.; Kaur, D.; Gupta, V. K. *J. Colloid Interface Sci.* **2010**, *343*, 463. [CrossRef]

[7] Dabrowski, A. *Adv. Coll. Interface Sci.* **2001**, *93*,135.

[CrossRef]

[8] Orthman, J.; Zhu, H. Y.; Lu, G. Q. *Sep. Purif. Technol.* **2003**, *31*, 53. [CrossRef]

[9] Fungaro, D. A.; Magdalena, C. P.; *Int. J. of Chem. Environ. Eng. Sci.* **2012**, *3*, 74.

[10] Ahmaruzzaman, M. Adv. Colloid and Interface Sci. **2011**, *166*, 36.

[11] Bhatnagar, A.; Sillanpää, M. *Chem. Eng. J.* **2010**, *157*, 277. [CrossRef]

[12] Gupta V. K.; Carrott, P. J. M.; Ribeiro-Carrot, M. M. L.; Suhas. *Crit. Rev. Environ. Sci. Technol.* **2009**, *39*, 783. [CrossRef]

[13] Gupta, V.K.; Suhas *J. Environ. Manage.* **2009**, *90*, 2313. [CrossRef]

[14] Fungaro, D. A.; Grosche, L. C.; Pinheiro, A. S.; Izidoro, J. C.; Borrely, S. I. *Orbital Elec. J. Chem.* **2010**, *2*, 235. [Link]

[15] Levandowski, J.; Kalkreuth, W. *Int. J. Coal Geol.* **2009**, *77*, 269. [CrossRef]

[16] Fungaro, D. A.; Bruno, M., Grosche, L. C. *Desalin. Water Treat.* **2009**, *2*, 231. [CrossRef]

[17] Cheriaf, M., Péra, J., Rocha, J. C. *Cem. Concr. Res.* **1999**, *29*, 1387. [CrossRef]

[18] Fungaro, D. A.; Silva, M. G. *Quim. Nova* **2002**, *25*, 1081. [CrossRef]

[19] Fungaro, D. A.; Flues, M. S-M; Celebroni, A. P. *Quim. Nova* **2004**, *27*, 582. [CrossRef]

[20] Fungaro, D. A.; Izidoro, J. C.; Almeida, R. S.; *Eclética Quim.* **2005**, *30*, 31. [CrossRef]

[21] Fungaro, D. A.; Izidoro, J. C. *Tchê Quím.* **2006a**, *3*, 21.

[22] Fungaro, D. A.; Izidoro, J. C. *Quim. Nova* **2006b,** *29*, 735. [CrossRef]

[23] Querol, X.; Moreno, N.; Umaña, J. C.; Alastuey, A.; Hernández, E.; López-Soler A.; Plana, F. *Int. J. Coal Geol.* **2002**, *50*, 413. [CrossRef]

[24] Rayalu, S. S.; Bansiwal, A. K.; Meshram, S. U.; Labhsetwar, N.; Devotta, S. *Catal. Sur. Asia* **2006**, *10*, 74. [CrossRef]

[25] Carvalho, T. E. M.; Fungaro, D. A.; Magdalena, C. P.; Cunico, P. *J. Radioanal. Nucl. Chem.* **2011**, *289*, 617. [CrossRef]

[26] Izidoro, J. C.; Fungaro, D. A.; Santos, F. S.; Wang, S. *Fuel Process Technol.* **2012a**, *97*, 38. [CrossRef]

[27] Izidoro, J. C.; Fungaro, D. A.; Wang, S. *Adv. Mater. Res.* **2012b**, *356-360*, 1900. [CrossRef]

[28] Fungaro, D. A.; Yamaura, M.; Carvalho, T. E. M. *J. At. Mol. Sci.* **2011**, *2*, 305.

[29] Fungaro, D. A.; Graciano, J. E. A. *Adsorpt. Sci. Technol.* **2007**, *10*, 729. [CrossRef]

[30] Henmi, T. *Soil Sci. Plant Nutr.* **1987**, *33*, 517. [CrossRef]

[31] Scott, J.; Guang, D.; Naeramitmarnsuk, K.; Thabuot, M. J. *Chem. Technol. Biotechnol.* **2002**, *77*, 63. [CrossRef]

[32] Shigemoto, N.; Hayashi, H.; Miyaura, K. *J. Mater. Sci.* **1993**, *28*, 4781. [CrossRef]

[33] Kreuz, A. L. Utilização de cinzas pesadas de termelétricas na substituição de cimento e areia na confecção de concretos. [Master's thesis.] Florianópolis, Brazil: Departamento de Engenharia Civil da Universidade Federal de Santa Catarina, 2002.

[34] Paprocki, A. Síntese de zeólitas a partir de cinzas de carvão visando sua utilização na descontaminação de drenagem ácida de mina. [Master's thesis.] Porto Alegre, Brazil, Pontifícia Universidade Católica do Rio Grande do Sul, 2009.

[35] Sijakova-Ivanova, T.; Panov, Z.; Blazev, K.; Zajkova-Paneva, V. *Int. J. Eng. Sci. Technol.* **2011**, *3*, 8219.

[36] Depoi, F. S.; Pozebon, D.; Kalkreuth, W. D. *Int. J. Coal Geol.* **2008**, *76*, 227. [CrossRef]

[37] Fungaro, D. A.; Borrely, S. I. *Ceram.* **2012**, *58*, 77 (in Portuguese with English abstract). [CrossRef]

[38] Umaña-Peña, J.C. Síntesis de zeolitas a partir de cenizas volantes de centrales termoeléctricas de carbón. [PhD Thesis.] Barcelona, Espanha, Universitat Politécnica de Catalunya, 2002.

[39] Ho, Y. S.; McKay, G. *Can. J. Chem. Eng.* **1998**, *76*, 822. [CrossRef]

[40] Ho, Y. S.; Wase, D. A. J.; Forstera C.F. *Environ. Technol* **1996**, *17*, 71. [CrossRef]

[41] Weber, W. J.; Morris, J. C. *Sanit J. Engin. Div., ASCE*, **1963**, *89*, 31.

[42] Allen, S. J.; McKay, G.; Khader, K.Y.H. *Environ. Pollut.* **1989**, *56*, 39. [CrossRef]

[43] Helby, W. A. *Chem. Eng.* **1952**, *59*, 153.

[44] Weber, W. J. Jr In: Weber W.J. Jr (ed) Physicochemical processes for water quality control, New York: Wiley-Interscience, 1972.

[45] Zou, W.; Zhao, L.; Han, R. *J. Radioanal. Nucl. Chem.* **2011**, *288*, 239. [CrossRef]

[46] Mall, I. D.; Srivastava, V. C.; Agarwal, N.; K.; Mishra, I. M. *Chemosphere* **2005**, *61*, 492. [CrossRef]

[47] Dubinin, M. M.; Radushkevich, L. V. *Proc. Acad. Sci. USSR Phys. Chem. Sect.* **1947**, *55*, 331.

[47] Giles, C. H.; MacEwan, T. H.; Nakhwa, S. N.; Smith, D. *J. Chem. Soc. London* **1960**, 3973.

[48] Helfferich, F. Ion Exchange; McGraw-Hill: New York, 1962.

[49] Giles, C. H.; Smith, D.; Huitson, A. *I. Theoretical. J. Colloid Interface Sci.* **1974**, *47*, 755. [CrossRef]

[50] Giles, C. H.; MacEwan, T. H.; Nakhwa, S. N.; Smith, D. *J. Chem. Soc. London* **1960**, 3973.

[51] Mohd Din, A.T.; Hameed, B. H. *J. Appl. Sci. in Environ. Sanitation* ***2010***, *5*, 161.

[52] Ho, Y. S., *Carbon* **2004**,42, 2115. [CrossRef]

[53] Ali, A. A.-H.; El-Bishtawi, R. *J. Chem. Technol. Biotechnol.* **1997**, *69*, 27. [CrossRef]

[54] Çoruh, S.; Geyikçi, F.; Nuri O. N. ATINER'S Conference Paper Series, Athens, Greece, 2012.

[55] Gandhimathi, R.; Ramesh S.T.; Sindhu, V., Nidheesh P.V. *Iran J. Energy & Environ.* **2012**, *3*, 52.

[56] Eren E.; Cubuk, O.; Ciftci H.; Eren, B.; Caglar, B. *Desalin.* **2010**, *252*, 88. [CrossRef]

[57] Malarvizhi, R.; Ho, Y. S. *Desalin.* **2010**, *264*, 97. [CrossRef]